ADVANCED FUNCTIONAL MATERIALS
www.afm-journal.de

Nitrogen-Doped Mesoporous Carbon Promoted Chemical Adsorption of Sulfur and Fabrication of High-Areal-Capacity Sulfur Cathode with Exceptional Cycling Stability for Lithium-Sulfur Batteries

*Jiangxuan Song, Terrence Xu, Mikhail L. Gordin, Pengyu Zhu, Dongping Lv, Ying-Bing Jiang, Yongsheng Chen, Yuhua Duan, and Donghai Wang**

As one important component of sulfur cathodes, the carbon host plays a key role in the electrochemical performance of lithium-sulfur (Li-S) batteries. In this paper, a mesoporous nitrogen-doped carbon (MPNC)-sulfur nanocomposite is reported as a novel cathode for advanced Li-S batteries. The nitrogen doping in the MPNC material can effectively promote chemical adsorption between sulfur atoms and oxygen functional groups on the carbon, as verified by X-ray absorption near edge structure spectroscopy, and the mechanism by which nitrogen enables the behavior is further revealed by density functional theory calculations. Based on the advantages of the porous structure and nitrogen doping, the MPNC-sulfur cathodes show excellent cycling stability (95% retention within 100 cycles) at a high current density of 0.7 mAh cm^{-2} with a high sulfur loading (4.2 mg S cm^{-2}) and a sulfur content (70 wt%). A high areal capacity (≈3.3 mAh cm^{-2}) is demonstrated by using the novel cathode, which is crucial for the practical application of Li-S batteries. It is believed that the important role of nitrogen doping promoted chemical adsorption can be extended for development of other high performance carbon-sulfur composite cathodes for Li-S batteries.

1. Introduction

Lithium-sulfur batteries have attracted increasing attention as next-generation energy storage devices for plug-in hybrid and all-electric vehicles, owing to the extremely high theoretical specific capacity (1672 mA h g^{-1}) and energy density (2600 Wh kg^{-1}) of sulfur.[1–6] In addition, sulfur is low-cost, abundantly available, and eco-friendly. Despite these considerable advantages, practical realization of a Li-S battery is hindered by several issues.[7–14] First, the low electrical conductivity of sulfur necessitates the use of a large amount of electrochemically inactive conductive carbon to improve utilization of the active materials, lowering overall cathode energy density. Second, the Li-S battery operates by reversible conversion of sulfur to different lithium sulfide products (Li_2S_x, $1 \le x \le 8$) through a multistep redox reaction. The electrolytes normally used in Li-S batteries have the ability to dissolve insulating polysulfides and thus improve their reaction kinetics. However, the dissolution of lithium polysulfides can also lead to loss of active material from the cathode and to a polysulfide shuttle phenomenon, resulting in capacity fading and poor coulombic efficiency. Third, high sulfur loading and content in cathodes generally make polarization more severe and lead to poor cycling stability, lower capacity, and decreased coloumbic efficiency.[15] However, as highlighted in the recent review on lithium-sulfur batteries,[16] sulfur cathodes would need to have a relatively high sulfur loading in order to achieve a higher capacity electrode than that of current lithium-ion batteries (2–4 mAh cm^{-2})[17–19] and a high sulfur content to achieve good volumetric capacity.

A variety of strategies have been explored to advance lithium-sulfur batteries, including design of novel cathodes (e.g., carbon-sulfur and conductive polymer-sulfur nanocomposites),[4–6,9,20–22] electrolytes (e.g., solid-state electrolytes and lithium-protecting electrolyte additives),[11,23–29] and separators (e.g., carbon interlayers).[30,31] The development of novel functional carbon with the ability to chemically adsorb sulfur

Dr. J. Song, T. Xu, M. L. Gordin, Dr. D. Lv, Prof. D. Wang
Department of Mechanical and Nuclear Engineering
The Pennsylvania State University
University Park, PA, 16802, USA
E-mail: dwang@psu.edu
P. Zhu, Prof. Y. Chen
EMS Energy Institute and Department of Energy and Mineral Engineering
The Pennsylvania State University
University Park, PA, 16802, USA
Dr. Y.-B. Jiang
Center for Micro-Engineered Materials
University of New Mexico,
Albuquerque, New Mexico, 87131, USA
Dr. Y. Duan
National Energy Technology Laboratory
United States Department of Energy
Pittsburgh, PA, 15236, USA

DOI: 10.1002/adfm.201302631

or lithium sulfide (Li_2S) is particularly attractive.[10] Chemisorption can enable uniform distribution of sulfur and Li_2S on carbon, thereby promoting good electrical contact, and can effectively confine polysulfides in the cathode by preventing dissolution.[10,32] Therefore, these reported functional carbon-sulfur cathodes show enhanced utilization of the active sulfur and excellent cycling stability compared with traditional carbon-sulfur composite cathodes that mainly rely on weaker physical adsorption of sulfur and lithium sulfide on carbon.[5,6,20,33,34] For example, Zhang and co-workers used graphene oxide as a conductive framework for sulfur, taking advantage of the chemical interaction between functional groups on graphene oxide and sulfur to help immobilize sulfur and thus efficiently improve the utilization of active materials and reduce the shuttle effect.[10] Archer and team reported a polyacrylonitrile (PAN)/Li_2S_3-based carbon-lithium sulfide composite utilizing the chemical interaction between the nitrile group and lithium polysulfides, yielding high galvanic charge/discharge capacities and excellent coulombic efficiency.[32]

Although these developments are encouraging, using functional carbon with chemical bonding capability as a sulfur host is still a challenge. Up to now, very few functional carbon materials have successfully been exploited as sulfur cathodes. Not all functional carbons can chemically bond with sulfur or Li_2S, and unique chemical structures are required to realize these strong interactions. Moreover, the fundamental understanding of the phenomenon, such as how and why these functional groups can interact with sulfur, is still lacking, especially on the molecular level.

While cathodes have been reported that take advantage of such behaviors to improve conductivity and mitigate polysulfide dissolution, most reports have paid little attention to areal capacity. Despite the improvement of specific capacity based on these strategies, the cathodes have a low sulfur loading (0.5–2 mg S cm^{-2}), leading to an areal capacity below 2 mAh cm^{-2}.[5,6,32,35–39] Thus, these sulfur cathodes are far from practical application even though they have extremely high theoretical capacity and energy density.

Herein, we report a novel mesoporous nitrogen-doped carbon (MPNC)-sulfur nanocomposite as a cathode material for Li-S batteries and demonstrate that the nitrogen doping can effectively induce chemical adsorption of sulfur on the high-surface-area carbon framework. To understand the mechanism behind the chemical adsorption, we did in-depth investigation by a combination of material characterization techniques such as X-ray absorption near edge structure spectroscopy (XANES) and theoretical simulation based on density functional theory. It was found that nitrogen doping promotes adsorption of sulfur on oxygen functional groups in the nitrogen-doped carbon framework. Taking advantage of the chemical adsorption for Li-S batteries, the MPNC-S cathodes show excellent coulombic efficiency (>96%) and cycling stability (95% retention within 100 cycles). More importantly, high areal capacity (3.3 mAh cm^{-2}) can be demonstrated by using the novel cathode material, as the composite can be fabricated into electrodes with high sulfur loading (over 4 mg S cm^{-2}) while maintaining a good capacity of around 800 mAh g^{-1}.

2. Results and Discussion

The synthesis of MPNC involves evaporation-induced multicomponent co-assembly of polymer precursor and labile porogens to form a mesostructured nanocomposite, followed by carbonization and removal of the porogens.[40,41] A commercial poly(melamine-co-formaldehyde) resin was selected as the polymer precursor and served as the carbon and nitrogen source, which makes large scale fabrication feasible. To get high pore volume and high surface area for sulfur loading and immobilizing, tetraethyl orthosilicate, amphiphilic triblock copolymers (Pluronic F127, $(EO)_{106}$-$(PO)_{70}$-$(EO)_{106}$), and colloidal SiO_2 nanoparticles (10–20 nm in diameter) were all used as porogens (see experimental section in the Supporting Information). X-ray photoelectron spectroscopy (XPS) was performed to probe the surface chemical composition of the MPNC (**Figure 1**a), showing the presence of C, N, and O atoms in MPNC. The binding energy peaks observed in the high-resolution N 1s profile at 397.8 eV and 400.3 eV (inset of Figure 1a) can be attributed to pyridinic and pyrrolic nitrogen, respectively.[42–45] The overall composition of the MPNC was investigated by elemental analysis (see Table S1 in Supporting Information).

The porous structure of MPNC was analyzed by transmission electron microscopy (TEM) (Figure S1, Supporting Information) and nitrogen sorption (Figure S2, Supporting Information). MPNC has a disordered mesoporous structure, a Brunauer-Emmett-Teller (BET) surface area of 824.3 m^2 g^{-1}, and a Barrett-Joyner-Halenda (BJH) pore volume of 1.38 cm^3 g^{-1}. The BJH pore size distribution shows that MPNC possesses hierarchical pore structures composed of 2–3 nm diameter mesopores templated from SiO_2 formed by the TEOS precursor, intermediate-sized (≈4–8 nm diameter) mesopores primarily from the block copolymer, and larger (≈10–20 nm diameter) mesopores from the colloidal SiO_2 nanoparticles.[41] Above all, the high surface area and pore volume obtained in MPNC are able to accommodate high sulfur loading into the porous conductive network and to provide more active sites for chemically immobilizing sulfur species.

The MPNC-sulfur nanocomposites were prepared by a melt-diffusion method. Typically, sulfur and MPNC were mixed by grinding and then heated at 155 °C for 10 h, causing the molten sulfur to flow into the pores of the MPNC. The resultant composite is denoted as MPNC-SX, where X is the weight percentage of sulfur in the composite. The pore volume and surface area in MPNC-S70 composite remarkably decreased after sulfur loading (see Figure S2 in Supporting Information), confirming that sulfur flowed into the pores of porous carbon. The adsorption of sulfur on carbon likely allowed the sulfur to be uniformly distributed within the framework.[5,10,20] After increasing sulfur content to 80 wt%, the MPNC-S80 composite shows characteristic diffraction peaks of sulfur in its XRD pattern (Figure S3, Supporting Information), indicating not all the sulfur was confined within the pores. The sulfur content in the composite was confirmed by thermogravimetric analysis (Figure S4, Supporting Information).

The MPNC-S70 nanocomposites were further characterized by TEM and electron energy loss spectroscopy (EELS) elemental mapping of carbon, nitrogen, and sulfur (Figure 1c-1f). All three maps were found to have similar intensity across the sample,

Adv. Funct. Mater. **2013**,
DOI: 10.1002/adfm.201302631

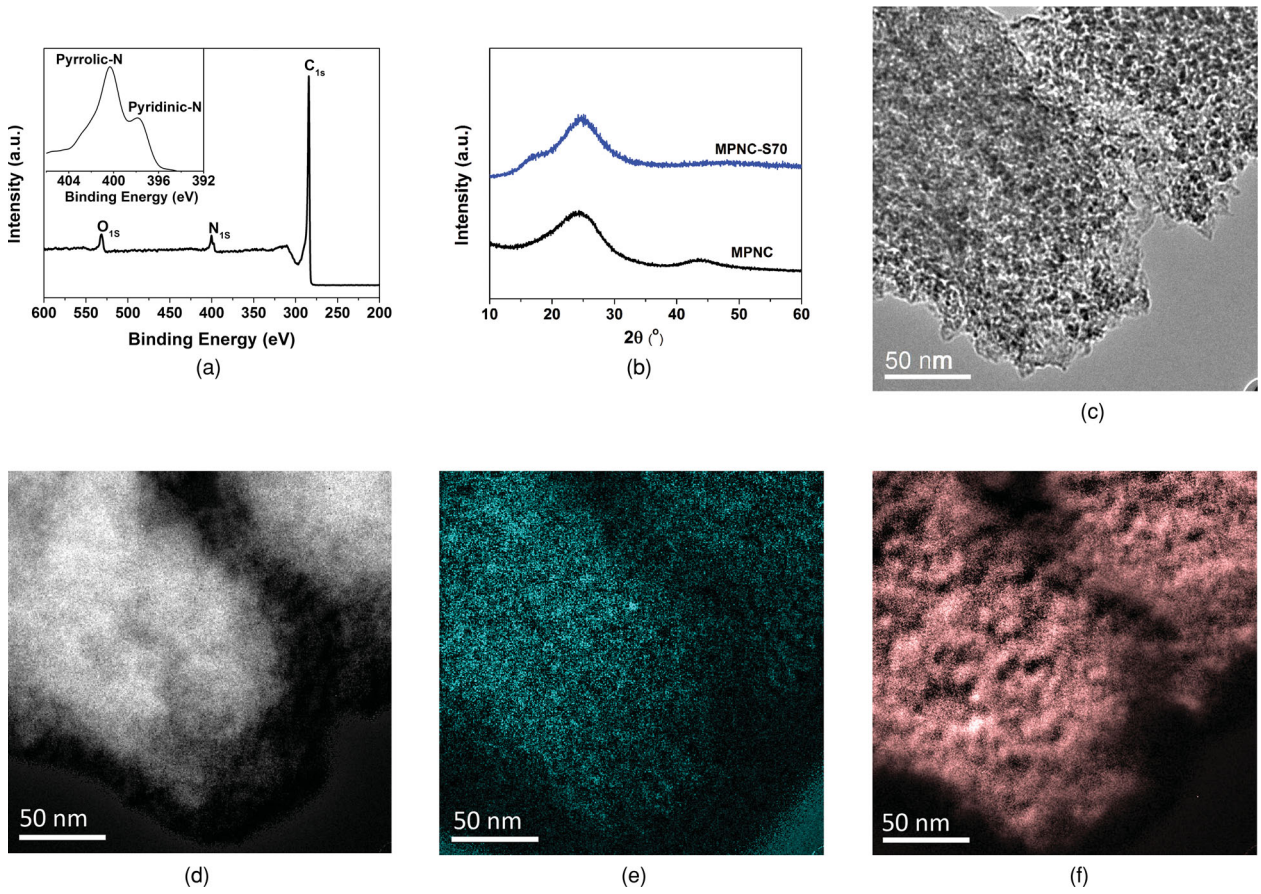

Figure 1. a) Main: XPS survey spectrum of MPNC. Inset: High-resolution spectrum of the N 1s peak. The peaks at 397.8 eV and 400.3 eV correspond to pyridinic and pyrrolic N, respectively; b) XRD patterns of MPNC and MPNC-S70; c) TEM image of an MPNC-S70 nanocomposite and corresponding EELS elemental maps of d) carbon, e) nitrogen, and f) sulfur.

besides the remarkably reduced pore volume and BET surface area of MPNC-S (see Figure S2, Supporting Information), indicating that nitrogen is evenly distributed throughout the carbon framework and confirming that sulfur is homogeneously impregnated into the small pores of the MPNC. The sulfur mapping is also consistent with the X-ray diffraction pattern of MPNC-S70 nanocomposite shown in Figure 1b, which has no observable reflection peaks of bulk sulfur.

Adsorption of sulfur on MPNC was first investigated by using XANES, as XANES is very sensitive to local coordination structure around a specific element of interest. Almost no changes are observed in the C and N coordination structures of MPNC after sulfur loading (Figure S5 in Supporting Information). However, there is a significant change in O coordination structure of MPNC after sulfur loading (**Figure 2**a). More ether-type oxygen functional groups and less carboxyl-type and/or carbonyl-type functional groups are present in MPNC-S compared with that in MPNC based on data fitting with reference compounds (see Table S2 in Supporting Information).[46] This indicates oxygen-sulfur bonding between carbonyl and carboxyl groups of MPNC and sulfur. We also observed a continuous line shift in oxygen XANES spectra with increasing the sulfur content within the measured sulfur loading range (Figure S6 in Supporting Information), which implies that more sulfur is accessible to the oxygen-containing functional groups as sulfur content increases. On the other

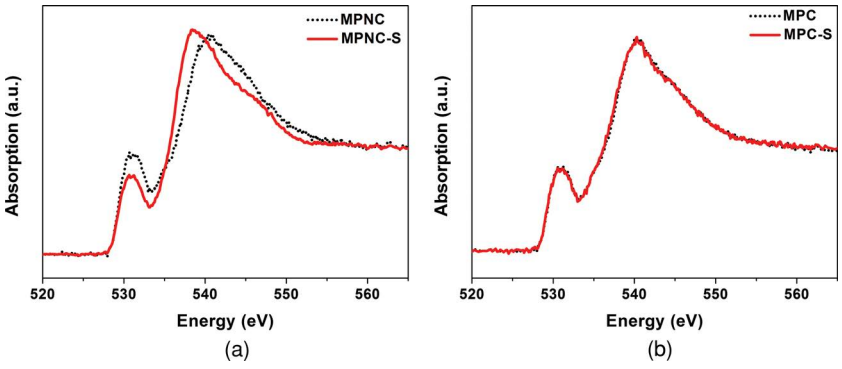

Figure 2. a) Oxygen K-edge XANES spectra of MPNC and MPNC-S nanocomposites; b) Oxygen K-edge XANES spectra of MPC and MPC-S nanocomposites.

hand, there are no obvious changes in the coordination structures of O and C in mesoporous carbon (MPC) with similar oxygen content after sulfur loading (Figure 2b, Figure S5 and Table S1 in Supporting Information), indicating that there is no significant chemical interaction between MPC and sulfur.

To better understand the mechanism by which nitrogen can promote oxygen-containing functional groups chemically bonding with sulfur, the DFT calculation was conducted. The detailed descriptions of our calculations are given in the Experimental Section. **Figure 3** and Figure S7 (Supporting Information) show the optimized structures of the sulfur adsorbed on –CO or –COOH groups in different types of N-doped carbon. The enthalpy changes (ΔH) of sulfur on the different carbon substrates were calculated as the energy differences between the adsorbed states and the separated substrates and sulfur atom adsorbate. **Table 1** summarizes the calculated ΔH of sulfur atom adsorbed on O and N of both N-doped and N-free carbon surface. The more negative value of ΔH indicates that the formation of the final product is more thermodynamically favorable. As one can see from Table 1, the ΔH of the carboxyl group of pyridinic-N-doped carbon (–56.88 kCal mol^{-1}) is the lowest in all three carboxyl groups of both the N-doped and N-free carbon, while the ΔH of the carbonyl group of pyrrolic-N-doped carbon is the overall lowest with a value of –117 kCal mol^{-1}. The lowest ΔH of sulfur adsorption on the oxygen functional groups of the N-doped carbon among different carbon surfaces indicates enhanced stabilization of sulfur on the nitrogen-doped carbon and that nitrogen-doping can facilitate the bonding of sulfur atoms with oxygen-containing functional groups. One can also observe in Table 1 that the interactions of sulfur with O on both pyridinic N–C**O**OH and pyrrolic N–C=O groups are stronger than that with N in all the functional groups, indicating that sulfur atoms prefer to bond with O rather than N. The DFT caculation results are consistent with the XANES results discussed above that S–O bond instead of N–S bond are formed based on oxygen and nitrogen K-edge XANES (Figure 2b and Figure S5c, Supporting Information) analysis. The spin density and charge distribution of carbon atoms will be influenced by the neighbor nitrogen dopants for nitrogen-doped carbon.[44,47,48] When nitrogen is doped into the carbon matrix, the nitrogen is electron deficient and acts as electron withdrawing atom due to the higher electronegativity of nitrogen (3.0) than carbon (2.5), causing the nearby oxygen containing groups (such as carbonyl and carboxyl groups) polarized and more easily attacked by the sulfur atom as the carbon and sulfur undergo high temperature (155 °C). Both XANES results and DFT calculation consistently confirm nitrogen doping in MPNC can change the electronic structure of nearby oxygen atoms in the doped carbon framework to promote the chemical interaction of the oxygen with sulfur.

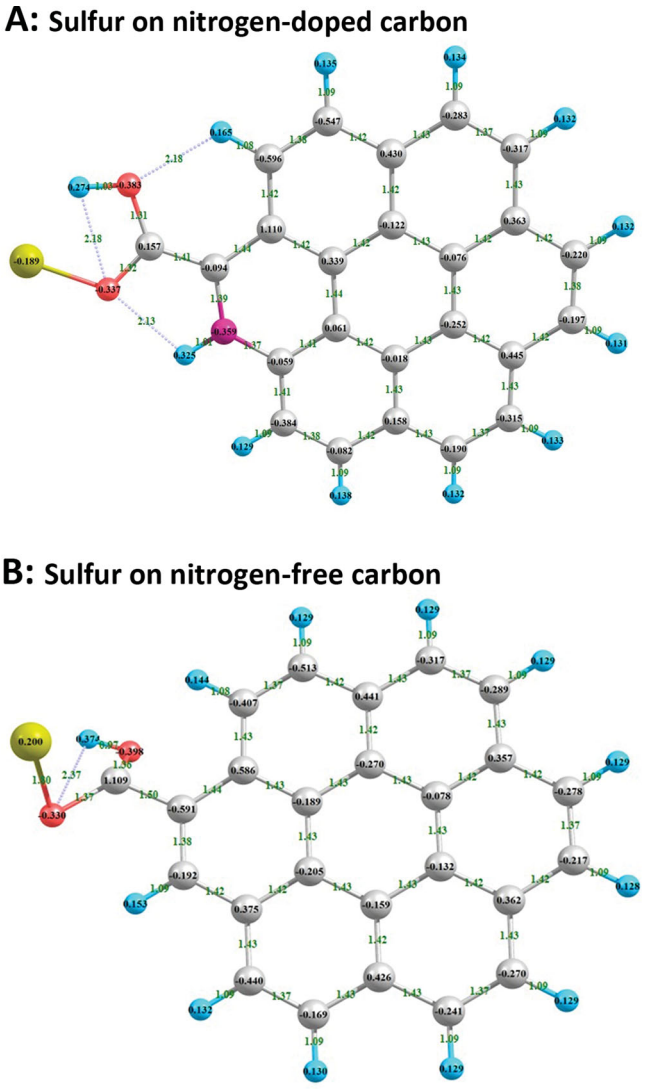

Figure 3. The top views of sulfur adsorbed on a) nitrogen doped carbon with pyridinic N_COOH functional group, and b) nitrogen-free carbon with –COOH group. The optimized bond-lengths and atomic charges are also shown. It was found that sulfur atom prefers to bond with O atom in –COOH groups in both nitrogen-doped and nitrogen-free carbon. The calculated interaction energies of sulfur on nitrogen-doped carbon and nitrogen-free carbon are –56.88 kCal/mol and –41.92 kCal mol^{-1}, respectively, indicating that nitrogen doping can enhance the stabilization of sulfur on –COOH group in the carbon. Yellow, red, magenta, silver gray and blue balls denote S, O, N, C, and H atoms, respectively.

Since MPNC shows strong chemical adsorption of sulfur, we expect that sulfur cathodes based on the functional carbon should have improved electrochemical performance. The

Table 1. DFT calculated interaction energies (ΔH, kCal mol^{-1}) of adsorbed sulfur atom on different active sites of nitrogen-doped carbon and nitrogen-free carbon.

	–COOH			–C = O			N			
Adsorbed site	Pyridinic N_COOH	Pyrrolic N_COOH	Nitrogen- free carbon_COOH	Pyridinic N_C = O	Pyrrolic N_C = O	Nitrogen-free carbon_C = O	Pyridinic N-COOH	Pyrrolic N-COOH	Pyridinic N-CO	Pyrrolic-N-CO
ΔH	–56.88	–49.00	–41.92	–59.02	–117.00	–106.09	–42.67	–50.85	–54.06	–111.80

Adv. Funct. Mater. **2013**,
DOI: 10.1002/adfm.201302631

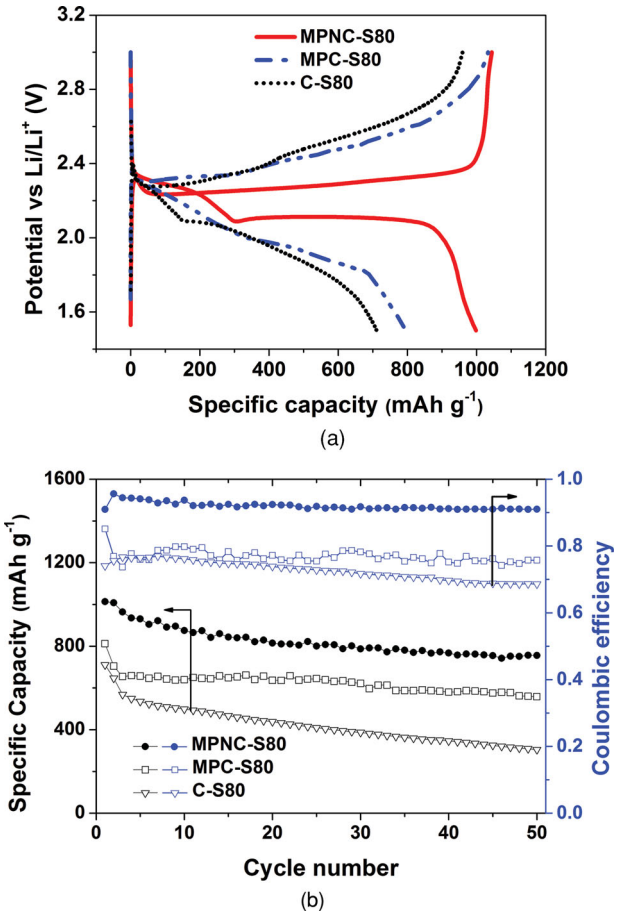

Figure 4. a) Initial discharge–charge voltage–capacity profiles and b) cycling performance and Coulombic efficiency of MPNC-S80, MPC-S80, and C-S80 cathodes at a current density of 0.18 mA cm^{-2}.

as-synthesized MPNC, together with the other two nitrogen-free carbon control samples (mesoporous carbon (MPC) and Super P carbon black), were studied as sulfur hosts. The corresponding electrodes with high sulfur content (80 wt%) were prepared using a melt-diffusion method and named as MPNC-S80, MPC-S80, and C-S80, respectively. The typical sulfur loading of these electrodes is ≈1.1 mg S cm^{-2} and the battery performance was studied in two-electrode CR2016 coin cells using a galvanostatic charge-discharge process with 1 M lithium bis(trifluoromethanesulfonyl)imide (LiTFSI) in 1,3-dioxolane/dimethoxy ethane (DOL/DME, 1:1 volume ratio) as the electrolyte. **Figure 4**a shows typical discharge-charge voltage profiles of MPNC-S80, MPC-S80, and C-S80 cathodes at a current density of 0.18 mA cm^{-2} between 1.5 and 3.0 V. The voltage profiles show distinct differences between MPNC-S80 and the control cathodes. Significant polarization was observed in the charge/discharge profiles of both MPC-S80 and C-S80 due to decreased conductivity of the cathodes. In contrast, MPNC-S80 still clearly shows discharge plateaus of 2.3 V and 2.1 V, indicating much less severe polarization at the high sulfur loading, which was further confirmed by the much lower charge transfer resistance observed in electrochemical impedance spectra of MPNC compared to those of MPC (see Figure S8 in Supporting Information). The initial discharge capacity of MPNC-S80 was 1013 mAh g^{-1} with a coulombic efficiency of over 90% as shown in Figure 4b. At the second cycle, a large reversible capacity of about 1008 mAh g^{-1} is obtained, corresponding to capacity retention of ≈99.5%, which is much higher than that of MPC-S80 (≈86.6%) and C-S80 (≈91.1%). The cycling stability of the MPNC-S80 electrode was good, with a high capacity retention of 80% within 50 cycles at 0.17 mAh cm^{-2}. In contrast, MPC-S80 and C-S80 show faster capacity fading and much lower coulombic efficiency. The difference in voltage profiles and coulombic efficiencies can be attributed to nitrogen-doping-induced chemical adsorption in MPNC-S80, which works in addition to the ability of the pores to contain sulfur. The chemical adsorption can facilitate uniform dispersion of sulfur during sulfur loading and uniform redeposition of sulfur during delithiation, thus decreasing charge transfer resistance and retarding diffusion of polysulfides away from the cathode. This is believed to be because the sulfur bonded to oxygen functional groups of the MPNC can easily bond to open sulfur atoms of sulfur chains, such as partly-delithiated polysulfides (i.e., LiS_x^-)[49,50] or S_x chains formed upon heating during sulfur loading.[37,51] The formation of sulfur chains bonded to the surface at the oxygen functional groups can further mitigate polysulfides to fully delithiate to free S_8 molecules and aggregate into large particles at the surface.

In order to demonstrate the potential of the MPNC-S composite cathode for practical use, MPNC-S70 (70 wt% S) cathodes with a high loading of 4.2 mg S cm^{-2} were fabricated. The sulfur content was slightly decreased in the fashion (from 80 wt% to 70 wt%) to ensure that sulfur was contained within the pores of the carbon framework and thus grant the electrode a higher conductivity. For electrochemical testing of these electrodes, lithium nitrate ($LiNO_3$, 0.2 M in electrolyte) was used as an electrolyte additive to further improve the coulombic efficiency, as $LiNO_3$ can protect the Li anode from reacting with soluble polysulfides.[24,52] **Figure 5**a shows a typical discharge–charge profile of an MPNC-S70 cathode at a current density of 0.35 mA cm^{-2} between 1.7 and 3.0 V. The discharge curve shows two plateaus at 2.3 V and 2.1 V versus Li/Li^+, corresponding to the reduction of sulfur to higher order lithium polysulfides (Li_2S_n, $6 \le n \le 8$) and the reduction of higher-order lithium polysulfides to lower-order lithium polysulfides (Li_2S_n, $2 \le n < 6$) and Li_2S, respectively.[6,53] The reverse reactions, corresponding to the oxidation of low order polysulfides and high order polysulfides, were displayed in the charge curve with two potential plateaus around 2.2 V and 2.4 V, respectively.[18] The cycle life and coulombic efficiency of the MPNC-S70 nanocomposite cathode are shown in Figure 5b. MPNC-S70 delivers an initial specific capacity of 1100 mAh g^{-1} and Coulombic efficiency of 99.4% at a current density of 0.35 mA cm^{-2}. The second cycle delivers a high reversible capacity of 990 mAh g^{-1}. After the first two activation cycles at 0.35 mA cm^{-2}, the cell was switched to 0.70 mA cm^{-2} for another 100 cycles. The capacity quickly stabilized at ≈800 mAh g^{-1} and showed roughly 95% retention within 100 cycles at a current density of 0.70 mA cm^{-2}. This loss of only 0.05% capacity per cycle is outstanding compared to cathodes in the existing literature. The high Coulombic efficiency (96–99%) of the MPNC-S70 nanocomposite is probably due to synergetic effects of both

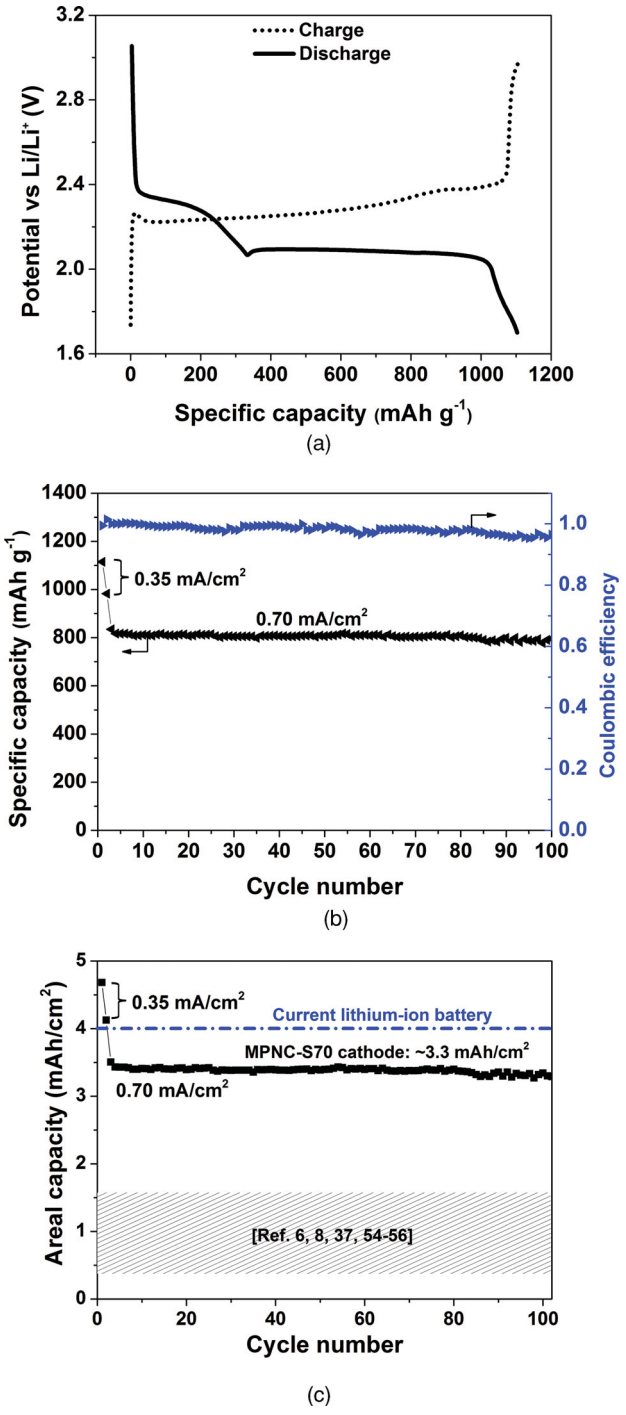

Figure 5. a) A typical first cycle discharge-charge voltage-capacity profile of an MPNC-S70 nanocomposite cathode at a current density of 0.35 mA cm^{-2}. b) Cycle performance and coulombic efficiency of MPNC-S70 cycled at a current density of 0.35 mA cm^{-2} for the first two cycles and 0.70 mA cm^{-2} for the subsequent cycles. The capacity values were calculated based on the mass of sulfur. c) The areal capacity of MPNC-S70 cathode with a sulfur loading of 4.2 mg S cm^{-2} and sulfur content of 70 wt%. The areal capacity is calculated by specific capacity (mAh g^{-2}) × sulfur loading (mg S cm^{-2}). The areal capacity of current lithium-ion battery is around 2–4 mAh cm^{-2}. The MPNC-S70 cathode shows an areal capacity of ≈3.3 mAh cm^{-2}, which is close to the high-end value of lithium-ion batteries. Areal capacity ranges of reported sulfur cathodes in references are also marked in grey.

the $LiNO_3$ additive and nitrogen-doping-induced chemical adsorption.

The areal capacity of MPNC-S electrodes is calculated as specific capacity (mAh g^{-1}) of sulfur × sulfur mass loading (g sulfur per centimeter of electrode face area). Based on this, it is clear that achieving a high areal capacity necessitates high sulfur loading in the electrodes. Most of the high specific capacities reported in the literature for electrodes fabricated by coating techniques were obtained at a low sulfur loading (below 2 mg S cm^{-2}) and/or low sulfur content (below 70 wt%).[6,8,37,54–56] The loading is insufficient to achieve a cathode with energy density greater than that of present Li-ion cathodes, as previously described. For the work, the MPNC-S cathode with a sulfur loading of 4.2 mg S cm^{-2} and high sulfur content of 70 wt% can deliver an areal capacity of 3.3 mAh cm^{-2} (Figure 5c), which is 2–10 times higher than other reports.[6,8,37,54–56] The areal capacity values estimated from recent publications are shown in the Li-S cell specific energy plot for comparison purposes.

3. Conclusion

In summary, we have developed a novel, mesoporous, nitrogen-doped carbon (MPNC)-sulfur nanocomposite as a cathode for Li-S batteries. The nitrogen doping in the MPNC material was found to promote formation of bonds between sulfur atoms and oxygen functional groups on the carbon, which is believed to play a key role in sulfur immobilization. The S–O chemical bonding was directly demonstrated by XANES, and the mechanism by which nitrogen enables the behavior was further revealed by DFT calculations. Based on the advantages of their structure and composition, the MPNC-S cathodes show excellent cycling stability at high current density of 0.7 mAh cm^{-2} with a high sulfur loading (4.2 mg S cm^{-2}) and sulfur content (70 wt%). The areal capacity of MPNC-S70 cathodes can reach ≈3.3 mAh cm^{-2}, which is superior to other reports. The novel nitrogen-doped carbon, as well as the related chemical adsorption mechanism, is very helpful for developing novel cathodes for lithium-sulfur batteries.

4. Experimental Section

Synthesis of Mesoporous Nitrogen-Doped Carbon (MPNC): MPNC was synthesized by using commercial poly(melamine-co-formaldehyde) resin (84 wt% solution in butanol) as the carbon precursor, with triblock copolymer Pluronic F127 ($PEO_{106}PPO_{70}PEO_{106}$), TEOS, and colloidal silica nanoparticles serving as poregens. The MF solution was diluted to 20 wt% MF by addition of ethanol before use. Typically, Pluronic F127 (1.6 g) was dissolved in a mixture of ethanol (15 mL) and HCl (0.2 M, 1.0 g) solution under continuous stirring at 40 °C to form a homogeneous solution. Then TEOS (2.08 g), colloidal silica latex (5 mL), and MF solution (5.0 g) were added in sequence. After being stirred for another 2 h, the final clear solution was transferred into petri dishes and the solvent was evaporated overnight in the fume hood at room temperature to produce transparent membranes. The membrane was further heated in an oven at 100 °C for 12 h and then 150 °C for 2 h to thermopolymerize the MF resin. Finally, the products were carbonized by heating them at 900 °C for 2 h in argon, with a temperature ramping rate of 1 °C min^{-1}, to obtain nitrogen-doped carbon-silica nanocomposites.

Adv. Funct. Mater. **2013**,
DOI: 10.1002/adfm.201302631

Silica was removed by immersing the nanocomposites in hydrofluoric acid solution (15 wt%) for 24 h at room temperature, yielding a three dimensional hierarchical MPNC.

Mesoporous carbon (MPC) is widely used as a conductive framework for sulfur cathodes. Herein, mesoporous carbon with similar surface area and pore volume to that of MPNC was selected as a control sample for our comparative study. The MPC was synthesized by an approach analogous to that used for MPNC by using phenolic resin as precursor according to publication by Zhao and co-workers.[34]

Characterization: The structure of the as-prepared composite was characterized by X-ray diffraction on a Rigaku Miniflex II spectrometer. X-ray photoelectron spectroscopy (XPS) measurements were carried out with a Kratos XSAM800 Ultra spectrometer. The surface morphologies of the composite particles were investigated with a JEOL JSM-2010 transmission electron microscope. Elemental mapping was performed with a TEM operating in Electron Energy Loss Spectroscopy (EELS) mode. Elemental analysis was performed by on a CHMS-OEA 1108 elemental analyzer. The surface area and pore structure were characterized by nitrogen sorption using a Micrometrics ASAP 2020 physisorption analyzer. The surface area was calculated by the Brunauer–Emmett–Teller (BET) method. The pore size distributions (Dp) were derived from the adsorption branches of isotherms using the Barrett–Joyner–Halenda (BJH) model. The content of sulfur in the composites was characterized by thermogravimetric analysis (TGA) at a temperature range of 25–600 °C with a heating rate of 10 °C min^{-1} under nitrogen atmosphere. The C (284.2 eV), N (409.9 eV), and O (543.1 eV) K-edge X-ray absorption near edge spectroscopy (XANES) spectra were collected in partial electron yield mode at beamline U7A of the National Synchrotron Light Source (NSLS) at Brookhaven National Laboratory. Maximum 5 wt.% of sulfur loading was applied to MPC and MPNC materials for XANES experiments due to the volatilization of sulfur species under ultra-high vacuum. The XANES spectra were processed and quantitatively analyzed using the ATHENA data analysis software via linear combination fitting.[57] Electrochemical impedance spectroscopy (EIS) measurement was performed using CHI 660D electrochemical workstation within the frequency range of 100 kHz to 10 mHz at potentiostatic signal amplitudes of 1 mV.

Electrode Film Preparation and Electrochemical Tests: The composite cathode was prepared by mixing 80 wt% composite powder, 10 wt% Super P, and 10 wt% polyvinylidene fluoride (PVDF) together in N-methyl-2-pyrrolidinone (NMP) to form a homogeneous slurry, then coating the slurry on aluminum foil. The electrodes were dried for two days at room temperature and then at 60 °C for 10 h under vacuum. In this work, the sulfur mass loading in MPNC-S70 electrodes is typically as high as 4–5 mg S cm^{-2} (4.20 mg S cm^{-2} for the electrode in Figure 5). Due to the higher polarization of MPNC-S80, MPC-S80, and C-S80 electrodes, the sulfur mass loading of these electrodes was lower, around 1.1 mg cm^{-2} (the sulfur loading of MPNC-S80, MPC-S80 and C-S80 in Figure 4 are 1.11 mg cm^{-2}, 1.13 mg cm^{-2}, and 1.05 mg cm^{-2}, respectively), in order to demonstrate the difference between the three electrodes (i.e., nitrogen doping effects) without $LiNO_3$ additives. The electrochemical performance of MPNC-S, MPC-S, and C-S was tested in a half-cell configuration using CR2016 type coin cells. The electrolyte was 1 M LiTFSI dissolved in a mixture of 1,3-dioxolane (DOL) and 1,2-dimethoxyethane (DME) (1:1 v/v), plus 0.2 M $LiNO_3$ for 70 wt% sulfur electrodes, and the separator was a microporous polypropylene membrane (25 µm thick, Celgard 2400). Cells were assembled in an argon-filled glove box and galvanostatically discharged and charged using a battery tester (Arbin BT-2000) at room temperature.

Computational Method: Similar to other theoretical studies on doped carbon systems,[58] in this study, we used coronene molecule to represent the carbon which contained 24 carbon atoms with 12 hydrogen atoms terminated at its edges. To simulate different types of nitrogen doping in carbon, we designed several models to capture the main environments of these N-doped carbon systems, as shown in Figure 3 and S7. All calculations were carried out by the first principles density functional theory implemented with Gaussian 09 software package[59] in a tight fit configurations. In the study, the B3LYP/6–31+G(d, p) level of computation was used for all structures to optimize geometries and to do the frequency calculations. Then, the electronic and thermal enthalpies of the systems studied are obtained. To obtain the binding energy of the sulfur adsorbed on N and O sites of the model, we take the energy difference between the energy of the absorbed system and the energies of the isolated sulfur atom and N-doped carbon. The charge distribution on each atom was evaluated based on Mulliken population analysis.

Supporting Information

Supporting Information is available from the Wiley Online Library or from the author.

Acknowledgements

J.S. and T.X. contributed equally to this work. This work was supported by the Assistant Secretary for Energy Efficiency and Renewable Energy, Office of Vehicle Technologies of the U.S. Department of Energy under Contract No. DE-EE0005475. The authors thank Dr. Daniel Fischer and Dr. Cherno Jaye for their help with the XANES measurements on U7A Beam-line at National Synchrotron Light Source.

Received: August 4, 2013
Published online:

[1] P. G. Bruce, S. A. Freunberger, L. J. Hardwick, J.-M. Tarascon, *Nat. Mater.* **2012**, *11*, 19.
[2] D. Wang, Q. Zeng, G. Zhou, L. Yin, F. Li, H.-M. Cheng, I. Gentle, G. Q. Lu, *J. Mater. Chem. A* **2013**, *1*, 9382.
[3] X. Ji, L. F. Nazar, *J. Mater. Chem.* **2010**, *20*, 9821.
[4] J. Schuster, G. He, B. Mandlmeier, T. Yim, K. T. Lee, T. Bein, L. F. Nazar, *Angew. Chem. Int. Ed.* **2012**, *51*, 3591.
[5] N. Jayaprakash, J. Shen, S. S. Moganty, A. Corona, L. A. Archer, *Angew. Chem. Int. Ed.* **2011**, *50*, 5904.
[6] X. Ji, K. T. Lee, L. F. Nazar, *Nat. Mater.* **2009**, *8*, 500.
[7] A. Manthiram, Y. Fu, Y.-S. Su, *Acc. Chem. Res.* **2013**, *46*, 1145.
[8] X. Ji, S. Evers, R. Black, L. F. Nazar, *Nat. Commun.* **2011**, *2*, 325.
[9] L. Xiao, Y. Cao, J. Xiao, B. Schwenzer, M. H. Engelhard, L. V. Saraf, Z. Nie, G. J. Exarhos, J. Liu, *Adv. Mater.* **2012**, *24*, 1176.
[10] L. Ji, M. Rao, H. Zheng, L. Zhang, Y. Li, W. Duan, J. Guo, E. J. Cairns, Y. Zhang, *J. Am. Chem. Soc.* **2011**, *133*, 18522.
[11] A. Hayashi, T. Ohtomo, F. Mizuno, K. Tadanaga, M. Tatsumisago, *Electrochem. Commun.* **2003**, *5*, 701.
[12] J. Nelson, S. Misra, Y. Yang, A. Jackson, Y. Liu, H. Wang, H. Dai, J. C. Andrews, Y. Cui, M. F. Toney, *J. Am. Chem. Soc.* **2012**, *134*, 6337.
[13] R. Demir-Cakan, M. Morcrette, Gangulibabu, A. Guéguen, R. Dedryvère, J.-M. Tarascon, *Energy. Environ. Sci.* **2013**, *6*, 176.
[14] C. Barchasz, F. Molton, C. Duboc, J.-C. Leprêtre, S. Patoux, F. Alloin, *Anal. Chem.* **2012**, *84*, 3973.
[15] S.-E. Cheon, K.-S. Ko, J.-H. Cho, S.-W. Kim, E.-Y. Chin, H.-T. Kim, *J. Electrochem. Soc.* **2003**, *150*, A800.
[16] S. S. Zhang, *J. Power Sources* **2013**, *231*, 153.
[17] M. S. Whittingham, *Chem. Rev.* **2004**, *104*, 4271.
[18] D. Aurbach, B. Markovsky, A. Rodkin, M. Cojocaru, E. Levi, H.-J. Kim, *Electrochim. Acta* **2002**, *47*, 1899.
[19] L. Hu, F. La Mantia, H. Wu, X. Xie, J. McDonough, M. Pasta, Y. Cui, *Adv. Energy Mater.* **2011**, *1*, 1012.
[20] C. Liang, N. J. Dudney, J. Y. Howe, *Chem. Mater.* **2009**, *21*, 4724.
[21] Y. Yang, G. Yu, J. J. Cha, H. Wu, M. Vosgueritchian, Y. Yao, Z. Bao, Y. Cui, *ACS Nano* **2011**, *5*, 9187.

[22] J. Kim, D.-J. Lee, H.-G. Jung, Y.-K. Sun, J. Hassoun, B. Scrosati, *Adv. Funct. Mater.* **2013**, *23*, 1076.
[23] J. Hassoun, B. Scrosati, *Adv. Mater.* **2010**, *22*, 5198.
[24] S. S. Zhang, *Electrochim. Acta* **2012**, *70*, 344.
[25] L. Suo, Y. S. Hu, H. Li, M. Armand, L. Chen, *Nat. Commun.* **2013**, *4*, 1481.
[26] J. H. Shin, E. J. Cairns, *J. Power Sources* **2008**, *177*, 537.
[27] E. S. Shin, K. Kim, S. H. Oh, W. I. Cho, *Chem. Commun.* **2013**, *49*, 2004.
[28] S. Chen, F. Dai, M. L. Gordin, D. Wang, *RSC Adv.* **2013**, *3*, 3540.
[29] Z. Lin, Z. Liu, W. Fu, N. J. Dudney, C. Liang, *Adv. Funct. Mater.* **2013**, *23*, 1064.
[30] Y.-S. Su, A. Manthiram, *Chem. Commun.* **2012**, *48*, 8817.
[31] Y.-S. Su, A. Manthiram, *Nat. Commun.* **2012**, *3*, 1166.
[32] J. Guo, Z. Yang, Y. Yu, H. D. Abruna, L. A. Archer, *J. Am. Chem. Soc.* **2013**, *135*, 763.
[33] J. Guo, Y. Xu, C. Wang, *Nano Lett.* **2011**, *11*, 4288.
[34] S.-R. Chen, Y.-P. Zhai, G.-L. Xu, Y.-X. Jiang, D.-Y. Zhao, J.-T. Li, L. Huang, S.-G. Sun, *Electrochim. Acta* **2011**, *56*, 9549.
[35] Y. Fu, Y. S. Su, A. Manthiram, *Angew. Chem. Int. Ed* . **2013**, *52*, 6930.
[36] W. Weng, V. G. Pol, K. Amine, *Adv. Mater.* **2013**, *25*, 1608.
[37] S. Xin, L. Gu, N.-H. Zhao, Y.-X. Yin, L.-J. Zhou, Y.-G. Guo, L.-J. Wan, *J. Am. Chem. Soc.* **2012**, *134*, 18510.
[38] C. Zhang, H. B. Wu, C. Yuan, Z. Guo, X. W. Lou, *Angew. Chem. Int. Ed* . **2012**, *51*, 9592.
[39] G. Zheng, Q. Zhang, J. J. Cha, Y. Yang, W. Li, Z. W. Seh, Y. Cui, *Nano Lett.* **2013**, *13*, 1265.
[40] Y. Deng, T. Yu, Y. Wan, Y. Shi, Y. Meng, D. Gu, L. Zhang, Y. Huang, C. Liu, X. Wu, D. Zhao, *J. Am. Chem. Soc.* **2007**, *129*, 1690.
[41] R. Liu, Y. Shi, Y. Wan, Y. Meng, F. Zhang, D. Gu, Z. Chen, B. Tu, D. Zhao, *J. Am. Chem. Soc.* **2006**, *128*, 11652.
[42] H. Wang, T. Maiyalagan, X. Wang, *ACS Catalysis* **2012**, *2*, 781.
[43] L. Qie, W. M. Chen, Z. H. Wang, Q. G. Shao, X. Li, L. X. Yuan, X. L. Hu, W. X. Zhang, Y. H. Huang, *Adv. Mater.* **2012**, *24*, 2047.
[44] W. H. Shin, H. M. Jeong, B. G. Kim, J. K. Kang, J. W. Choi, *Nano Lett.* **2012**, *12*, 2283.
[45] L. Sun, L. Wang, C. Tian, T. Tan, Y. Xie, K. Shi, M. Li, H. Fu, *RSC Adv.* **2012**, *2*, 4498.
[46] K. Kim, P. Zhu, N. Li, X. Ma, Y. Chen, *Carbon* **2011**, *49*, 1745.
[47] L. G. Bulusheva, A. V. Okotrub, A. G. Kurenya, H. Zhang, H. Zhang, X. Chen, H. Song, *Carbon* **2011**, *49*, 4013.
[48] L. Zhang, Z. Xia, *J. Phys. Chem. C* **2011**, *115*, 11170.
[49] Z. Lin, Z. Liu, W. Fu, N. J. Dudney, C. Liang, *Angew. Chem. Int. Ed.* **2013**, *52*, 7460.
[50] J. Wang, J. Yang, C. Wan, K. Du, J. Xie, N. Xu, *Adv. Funct. Mater.* **2003**, *13*, 487.
[51] B. Meyer, *Chem. Rev.* **1976**, *76*, 367.
[52] D. Aurbach, E. Pollak, R. Elazari, G. Salitra, C. S. Kelley, J. Affinito, *J. Electrochem. Soc.* **2009**, *156*, A694.
[53] L. X. Yuan, J. K. Feng, X. P. Ai, Y. L. Cao, S. L. Chen, H. X. Yang, *Electrochem. Commun.* **2006**, *8*, 610.
[54] J. Schuster, G. He, B. Mandlmeier, T. Yim, K. T. Lee, T. Bein, L. F. Nazar, *Angew. Chem. Int. Ed.* **2012**, *51*, 3591.
[55] Y. M. Lee, N.-S. Choi, J. H. Park, J.-K. Park, *J. Power Sources* **2003**, *119–121*, 964.
[56] S. Zhao, C. Li, W. Wang, H. Zhang, M. Gao, X. Xiong, A. Wang, K. Yuan, Y. Huang, F. Wang, *J. Mater. Chem. A* **2013**, *1*, 3334.
[57] B. Ravel, M. Newville, *J.Synchrotron Radiat.* **2005**, *12*, 537.
[58] S. S. Yu, W. T. Zheng, Q. B. Wen, Q. Jiang, *Carbon* **2008**, *46*, 537.
[59] S. Gong, Y. Chen, J. Luo, C. Yang, C. Zhong, J. Qin, D. Ma, *Adv. Funct. Mater.* **2011**, *21*, 1168.

Adv. Funct. Mater. **2013**,
DOI: 10.1002/adfm.201302631